Geochimica et Cosmochimica Acta 368 (2024) 12–23

Contents lists available at ScienceDirect

Geochimica et Cosmochimica Acta

journal homepage: www.elsevier.com/locate/gca

Lipid composition, caloric content, and novel oxidation products from microbial communities within seasonal pack ice cores

Henry C. Holm [a,b,*], Helen F. Fredricks [a], Shavonna M. Bent [a,b], Daniel P. Lowenstein [a,b], Kharis R. Schrage [a,b], Benjamin A.S. Van Mooy [a]

[a] Marine Chemistry and Geochemistry Department, Woods Hole Oceanographic Institution, Woods Hole, MA 02543, USA
[b] MIT-WHOI Joint Program in Oceanography/Applied Ocean Science & Engineering Cambridge, MA 02139, USA

ARTICLE INFO

Associate editor: Elizabeth Ann Canuel

Keywords:
Sea Ice
Lipidomics
FAHFA-TAG
Antarctica
Algae

ABSTRACT

Sea ice is a critical feature of polar environments with importance for coastal ecosystems. Along the West Antarctic Peninsula (WAP), climate change is causing decreases in seasonal sea ice duration and extent. Organic carbon within sea ice is an important aspect of southern ocean carbon cycling but less studied than water column or sedimentary carbon reservoirs. Though conditions within sea ice can be extreme, phytoplankton are able to flourish and serve as a key food source for higher trophic levels, especially in the spring and fall. A portion of this sea ice phytoplankton biomass is composed of lipids, which are both calorically dense and useful as tracers of biological processes within the sea ice. To better understand both the trophic value and the diversity of lipids present within sea ice we employed high-resolution accurate-mass mass spectrometry to analyze ice core samples from six sites collected along the peninsula in November 2018. Using untargeted methods we annotated 1,173 intact lipid species across 14 classes of intact polar lipids, triacylglycerols, and pigments. We compared lipids' physical distribution within sea ice cores and found they are highly geographically and physically heterogenous within sites. Ratios between intact polar lipid classes show little signs of phytoplankton nutrient stress; a finding consistent with internally nutrient replete sea ice brines. We found key differences in the composition between pack ice versus fast ice and observed chlorophyll *a* to be inconsistently correlated with triacylglycerol content. We determined the mean caloric content of lipids within pack ice (4.45 ± 3.47 kJ m^{-2}) and found that caloric densities from the lipids alone were in the range of total water column energy content. Lastly, we show evidence of fatty acid hydroxy fatty acid triacylglycerols within the ice matrix and discuss possible biochemical sources of these novel biomarkers in an ocean system. These results shed light on the chemical diversity of a dynamic and ecosystem relevant carbon pool.

1. Introduction

Antarctic sea ice constitutes a massive ecosystem covering 19×10^6 km^2 of ocean water at its greatest extent during the austral winter (Arrigo, 2014). The free floating non-landfast sea ice that forms and degrades annually (often referred to as "pack ice") in the Southern Ocean provides a valuable yet extreme environment for phytoplankton growth (Thomas, 2002). Sea ice associated primary production, while a small fraction of total net primary production within the southern ocean seasonal ice zone (~5%), plays an important role as a food source for both pelagic and benthic communities (Lizotte, 2001; Arrigo, 2017). During the winter-spring transition when water column primary production rates are still below summer peaks, many zooplankton species rely on phytoplankton biomass released during sea ice melting for their nutritional needs (Jia et al., 2016; Kohlbach et al., 2017). With spring melting, this sea ice biomass can also be a valuable food source for benthic communities as pulses of sinking organic matter from sea ice make their way to the seafloor (Wing et al., 2012). Sea ice algae seeded into the water column post melt can effect coastal carbon cycling by spurring blooms that may also become a food source (Schmidt et al., 2018). Growth conditions can have a large effect on organic carbon composition within phytoplankton, however, most devote around a third of their biomass to lipids (Bernaerts et al., 2019). Lipids are of great value for higher trophic levels on an energy density basis; lipid stores can have double the energy per gram compared to carbohydrate stores (Subramanian et al., 2013).

* Corresponding author.
E-mail address: hholm@whoi.edu (H.C. Holm).

https://doi.org/10.1016/j.gca.2024.01.003
Received 11 May 2023; Accepted 2 January 2024
Available online 5 January 2024

Phytoplankton growing within sea ice must adapt to extreme gradients in light, temperature, salinity, and nutrient availability across seasonal transitions. During the onset of winter, pack ice is seeded by water column phytoplankton, which must contend with high salinity (up to 100 PSU) created by salt exclusion from freezing water within the ice brine channels (Gleitz et al., 1995). Conversely, spring melting may expose phytoplankton transiently to hyposaline waters (<10 PSU) created from freshwater ice inputs (Ralph et al., 2007). While inorganic nutrients are initially concentrated into sea ice during freezing, nutrient levels within physically isolated ice brines can become limiting to microbial communities as concentrations are largely dependent on physical resupply and biological regeneration (Kuosa and Kaartokallio, 2006). Light exposure follows similar extremes for surface sea ice with little to no available radiation in the winter followed by high average exposure in the spring (Meiners et al., 2012).

Across the winter-spring transition, phytoplankton must change their metabolic strategy from relying principally on energy stores to photosynthetic growth and must contend with the associated oxidative stress (Sackett et al., 2013; Bowman et al., 2021). Photosynthesis in high light conditions risks production of excess radical oxygen species (ROS) that can threaten cell machinery (Foyer, 2018). Phytoplankton have multiple biochemical strategies for dealing with this oxidative stress including antioxidant accessory pigments and enzymes capable of reducing ROS (Wang et al., 2009; Foyer, 2018). However, excessive ROS can damage cellular membrane lipids. For example, ROS may cause the formation of hydroxy fatty acids, either through direct attack by ROS on lipid fatty acid unsaturations or mediated by a lipid specific peroxidase enzyme (Fontana et al., 2007; Ivanov et al., 2010; Collins et al., 2018). Recent work in Arctic sea ice examining fatty acids during the spring transition implicated enzymatic bacterial oxidation of lipids as the major source of degradation (Rontani et al., 2018). Production and fate of these potentially detrimental hydroxy fatty acids within polar phytoplankton, as well as novel compounds related to them, is an area of active research.

To better understand environmental pressures on microbial communities, the chemical diversity of production within sea ice, and its value to higher trophic levels, we characterized the lipid composition of 15 sea ice cores from coastal areas of the WAP during late spring conditions. We used high performance liquid chromatography (HPLC) coupled with electrospray ionization (ESI), high resolution accurate-mass spectrometry (HRAM-MS), and software tools to analyze 1,173 lipid species within ice core samples. We found lipid concentrations within the pack ice to be highly variable with some consistent patterns across cores and sites. We found that energy storage lipids triglycerides (TAGs) and membrane intact polar lipids (IPLs) contributed about equally to core caloric content with indications from correlation analyses that these pools are likely cycled differently within the ice. Lastly, within the TAG pool, we detected fatty acyl esters of hydroxy fatty acids in triglycerides (FAHFA-TAGs) that could be an indicator of a novel biochemical response to oxidative stress within the sea ice environment.

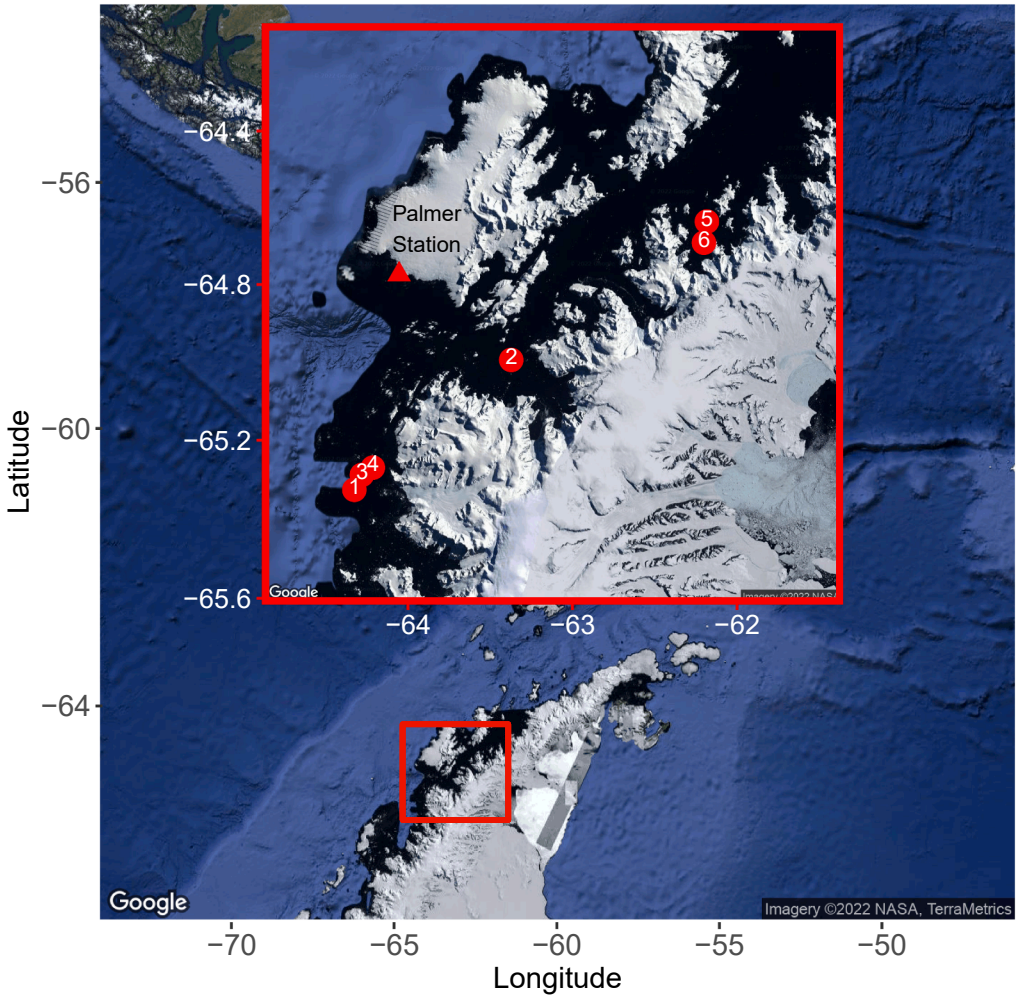

Fig. 1. Map of ice floe sampling sites on the West Antarctic Peninsula. Inset shows magnification of region bounded by red box. Sites are numbered with red dots indicating the locations of ice floes sampled. The location of Palmer Station is shown with a red triangle.

2. Methods

2.1. Sample collection and at sea processing

We collected samples at a total of six sites distributed between Grandidier Channel, Flandres Bay, and Wilhelmina Bay, all approximately 50–100 km from the US Antarctic program Palmer Station. Sampling was done during the 2018 research cruise LMG1810 aboard the research ship *R/V Laurence M. Gould* (Fig. 1, Table S1). Five sites (1–5) were sampled from free floating pack ice either in bays (Sites 2, 5) or in open waters of the Grandidier Channel (Sites 1, 3, 4). The ice cores were believed to come from first year sea ice as they were free floating and mostly less than 100 cm thick. We also obtained a single core from land fast sea ice along the coast of a northern bay in the Gerlache Strait (Site 6) which was possibly multiyear fast ice given its attachment to land away from the sea ice edge and the thickness of the ice (150 cm). We cored the entirety of the ice floe from the surface to the underside of the ice sheet. Variability in core length at each site derived from an uneven profile of the ice floes likely due to breaking and melting before our arrival. Samples were collected using a 9 cm diameter ice corer (Kovacs Mark II). Between 1 and 3 cores were taken at each site separated by 5–10 m for a total of 15 cores across all six sites (Table 1, Table S1). Cores were wrapped in black plastic and stored in dark containers for transport between ice sampling sites and the ship to avoid exposure to light after collection. In the laboratory under subdued light, collected cores were sectioned with an ice saw and submerged in buckets containing 500 mL of filtered (1 μm Whatman Polycap) seawater pumped from the ships underway system. Cores were segmented, on average, into nine depths yielding 142 individual samples for lipidomic analysis. Field blanks consisted of buckets containing only 500 mL of filtered seawater with no ice added. Ice core sections were place in the dark and allowed to melt in filtered seawater at ambient outdoor air temperature (0–5 °C) until all sections were completely melted (usually 48 h). However, cores from sites 4 and 5 melted much more rapidly as smaller sections of ice were melted from each core (1 h melt time). The volume of water yielded from each core section was highly dependent on the length and ice density of each subsample and ranged from 50−980 mL. The total volume of the melt for each core section was measured and a subset was filtered at 10 bar onto 0.22 μm hydrophilic PVDF-filters (Durapore Millipore Sigma), and flash frozen in liquid nitrogen (−196 °C). Filters were shipped to Woods Hole laboratory on dry ice (−78.5 °C) and stored in a −80 °C freezer before extraction.

Table 1
Caloric content of sea ice profiles. Values indicate means of replicate cores followed by the standard deviation.

Site	Ice Cores *n*	TAGs kJ m^{-2}	Chl *a* kJ m^{-2}	IPLs kJ m^{-2}	All Lipids kJ m^{-2}
1	3	5.18 ± 1.94	0.49 ± 0.26	3.91 ± 2.69	9.65 ± 3.47
2	3	1.49 ± 0.96	0.55 ± 0.25	1.32 ± 0.3	3.36 ± 1.13
3	3	2.89 ± 1.53	0.22 ± 0.1	0.92 ± 0.26	4.04 ± 1.88
4	2	0.36 ± 0.44	0.29 ± 0.21	0.99 ± 0.67	1.63 ± 1.32
5	3	2.34 ± 2.11	0.16 ± 0.14	0.13 ± 0.08	2.63 ± 2.28
6	1	0.18 ± NA	0.19 ± NA	0.11 ± NA	0.48 ± NA
Pack Ice (Sites 1–5)	14	2.6 ± 2.1	0.35 ± 0.23	1.49 ± 1.75	4.45 ± 3.47
All Cores (Sites 1–6)	15	2.44 ± 2.12	0.33 ± 0.23	1.4 ± 1.72	4.18 ± 3.5

2.2. Lipid extraction

We extracted filters with a modified Bligh and Dyer method following previously established extractions for lipidomic samples (Popendorf et al., 2013). In brief, filters were added to a combination of 0.8 mL of phosphate buffered saline (Fisher Scientific), 2 mL methanol, and 2 mL dichloromethane in two steps (0.8:2:1 *v:v:v*, 1:0:1 *v:v:v*). Samples were sonicated for 10 min with a FS110 sonicator bath (Fisher Scientific) after addition of the first solvents. Each sample received 10 μL of 1.5 mM butylated hydroxy toluene to reduce the risk of oxidation during processing or storage. Multiple deuterated internal standards were added to track recovery (Table 2). In addition to deuterated standards, 1,2-dipalmitoyl-sn-glycero-3-phosphoethanolamine-N-(2,4-dinitrophenyl) (DNP-PE) was added to track recovery of TAGs and Chl *a*. A dichloromethane total lipid extract (TLE) was retained and sealed under argon gas at −20 °C until analysis. Immediately before analysis, samples were dried under nitrogen gas and resuspend in acetonitrile/isopropanol (70:30 v:v).

2.3. HPLC-ESI-HRAM-MS analysis

We applied high performance liquid chromatography (HPLC) in tandem with electrospray ionization high resolution accurate mass (ESI-

Table 2
External and internal standards used for quantification and recovery of lipid classes.

Standard	Supplier	Used to Quantify (External)	Peak Area / pmolOC	Used for Recovery Calculation (Internal)
DNP-PE	Avanti Polar Lipids	*N/A*	68,483,874	Chlorophyll *a*, FAHFA-TAG, TAG
DGTS-d9	Avanti Polar Lipids	DGTS, DGTA, DGCC	280,770,306	DGTS, DGTA, DGCC
15:0–18:1 PE-d7	Avanti Polar Lipids	PE	51,415,477	PE
15:0–18:1 PC-d7	Avanti Polar Lipids	PC	62,035,362	PC
16:0–18:1 PG-d5	Avanti Polar Lipids	PG	19,821,035	PG
MGDG 36:0	Avanti Polar Lipids	MGDG	78,340,912	*N/A*
SQDG 34:3	Avanti Polar Lipids	SQDG	57,978,568	*N/A*
DGDG 36:0	Avanti Polar Lipids	DGDG	66,287,302	*N/A*
TAG Mix (See Table S3).	Avanti Polar Lipids, NuCheck Prep	TAGs	*Variable. See* Fig. S1	*N/A*
1-Palmitoyl-2–12-PAHSA-3-Oleoyl-sn-glycerol (FAHFA-TG)	Cayman Chemical	FAHFA-TAG	128,337,308	*N/A*
Chlorophyll *a*	Frontier Scientific	Chlorophyll *a*, Pheophytin *a*	47,289,154	*N/A*
C15 Glucosyl (β) Ceramide-d7	Avanti Polar Lipids	*N/A*	103,261,223	MGDG, DGDG, SQDG

HRAM) spectrometry for analysis of lipid species present in the ice core samples. We used reverse phase chromatography with a 5 μm particle size XBridge C8 column (2.1 mm inner diameter and 150 mm length, Waters Corporation) on a 1200 HPLC system (Agilent Technologies). A 20 μL injection of the TLE was used for analysis of each sample. The aqueous eluent consisted entirely of Milli-Q purified water (Millipore Sigma) while the organic eluent consisted of acetonitrile/isopropanol (70:30 v:v). Both solvents also received 1 % 1 M ammonium acetate and 0.1 % acetic acid by volume to aid in the creation of adducts in both negative and positive ESI modes. The HPLC was kept at a flow rate of 0.4 mL min^{-1} for the entire analysis. HPLC analysis used an eluent gradient starting with 45:55 ratio mixture of aqueous:organic eluents and ending with a 1:99 ratio after 15 min. This was followed by a 15 min hold at 1:99 for the remainder of acquisition. The voltage of the ESI source was 4.5 kV positive/3.0 kV negative. The temperatures were 200 °C and 350 °C for the capillary and ESI probe respectively.

Mass spectra were captured using a Themo Scientific Q-Exactive orbitrap mass analyzer. Samples were analyzed with alternating positive and negative mode full scans (200–1500 *m/z*) along with data-dependent MS/MS scans of the top three ions in each mode after every scan. Masses for MS/MS were isolated using a 4 *m/z* window. We used a resolution setting of 140,000 (FWHM at 200 *m/z*) and 17,500 for full scan and MS/MS scans respectively. We used a stepped combined normalized collision energy (NCE) of 30 %, 50 %, and 80 % to give a wide range of fragments. Four lock masses were used to maintain mass accuracy throughout the run in both modes: three polysiloxanes in positive mode (536.16591 *m/z*, 610.18416 *m/z*, and 684.20350 *m/z*) and a C19 free fatty acid (297.27990 *m/z*) in negative mode.

Subsequent analysis of three ice core samples for targeted identification of FAHFA-TAG species used identical HPLC conditions but different MS acquisition to get more complete MS/MS spectra from peaks of interest. Scanning was done exclusively in positive mode with one MS scan from 1000 to 1200 *m/z* followed by three data-dependent MS/MS scans using 10 % NCE. This was followed by an identical MS scan (1000–1200 *m/z*) and three MS/MS scans using 30 % NCE. Lastly, a single MS scan from 200 to 2000 *m/z* was used to monitor non-target ions.

2.4. Lipidomic annotation generation

We annotated lipids by using the R package LOBSTAHS which utilizes prescreening by the popular packages xcms and CAMERA (Benton et al., 2008; Kuhl et al., 2012; Collins et al., 2016). Full processing methods in the pipeline are detailed by Collins et al. (2016). Briefly, chromatographic peaks were detected at 5 ppm accuracy using the 'centWave' algorithm. Peaks were grouped using a density function and retention time corrected using the 'loess' method. Peaks not initially detected for a sample in each peak group were reintegrated from the raw mass spectral data to check presence. CAMERA was used to group peak groups into larger "pseudospecta" groups likely originating from the same feature. We lastly used the LOBSTAHS package to annotate compounds within a 5 ppm mass accuracy of entries in our *in-silico* lipid database (See Collins et al., 2016 for IPL compound classes included in database). Annotated compounds were validated using a combination of MS/MS fragmentation spectra, retention time patterning, adduct hierarchies, and positive–negative ionization patterns.

2.5. Quantification and response correction

Intact polar lipids were quantified from their peak areas to on-column molar amounts using external linear standard curves of representative lipid species (Table 2). This method has been validated for matrix and in-sample effects previously by our lab (Becker et al., 2018). Additionally, we used class specific deuterated internal standards to account for recovery efficiency and calculate the amount of lipid per liter of ice (Table 2). This is calculated as:

$$pmol\ L^{-1} = \frac{(PA \times RF)\frac{IS_{spk}}{IS_{rec}}}{Ice_{vol}}$$

where *PA* is the peak area of the annotated lipid, *RF* is the response of the lipid standard (pmol PA^{-1}), IS_{spk} is the mass of internal standard spiked in the sample, IS_{rec} is the amount recovered, and Ice_{vol} is the volume of ice melt filtered in liters. All lipid classes were quantified in positive ionization mode. Limits of quantification were determined using prediction intervals of standard curves as in Popendorf et al. (2013). All lipid quantities in ice core samples were blank subtracted using a field blank. Overall lipid levels in our field blank were very low and consisted mostly of PE and TAG species. After blank subtraction total lipid mass in ice core samples only shifted 1.2 % ± 1.8 % on average. However, in blanks of extraction solvents, saturated TAGs were significantly elevated among TAGs relative to their quantities in ice core samples (Kruskal-Wallis test, $p < 0.001$). Out of an abundance of caution, annotations for fully saturated TAGs were not considered in quantified TAG totals as they additionally only made up a small percent (average of 0.6 % ± 3.6 %) of TAG peak area across all samples..

For polar lipids, ionization of the headgroup most significantly affects the ionization response of the lipid species leading to a variability of no more than 20 % between species of high and low unsaturation (Popendorf et al., 2013). However, TAGs are more significantly affected by unsaturation differences and require a more robust response correction (Han and Gross, 2001; Holčapek et al., 2005). Due to this, we calculated the mass of TAGs in each sample as above but modeled the RF for each TAG species individually (Fig. S1, Table S3). As in previous studies, our lab has observed that the relative response of triglycerides was positively correlated with more fatty acid unsaturations and negatively correlated with carbon number (Becker et al., 2018). However, we observed that triglycerides below 42 fatty acid carbons were positively correlated with carbon number. Similar to Han and Gross, 2001, we predicted the relative response of various triglycerides of different unsaturation levels and carbon numbers by least-squares regression curve fitting of a model. We used the response of triglyceride standards measured in this study as well as in previous studies in our lab (Becker et al., 2018; Holm et al., 2022). We choose to use a formula of the form:

$$RRF = \beta_1 C^2 + \beta_2 C + \beta_3 \sqrt{U} + \beta_4$$

where *RRF* (relative response factor) is the response factor of a TAG standard relative to the DNP-PE standard, *C* is the number of carbon atoms in the fatty acid chains, and *U* is the number of unsaturations on the fatty acid chains. By modeling RRF rather than the RF we were able to compare TAG standards from separate batches and use consistent coefficients (β) for all analyses. All terms in the model were significant ($p < 0.001$) and predicted standard RRFs well ($R^2 = 0.83$, $p < 0.001$). The model had a root mean squared error (RMSE) of 0.754 and relative root mean squared error (i.e. the RMSE where the residuals are scaled against the actual RFFs) of 24 % putting it close to the likely error in the response factors of IPLs. The limit of quantification for TAGs was determined from the mean of the limits for seven TAG standard curves run with this study.

2.6. GC–MS analysis

We analyzed a subset of samples by GC–MS to evaluate the presence of highly branched isoprenoids (HBIs) in our ice cores. The sample with the highest Chlorophyll *a* value from each site was chosen for HBI analysis. From each total lipid extract, 20 % was removed (400 μL) and 5 μL of 7-hexaoctadecane (7-HOD, Sigma-Aldrich, 25 ng/L) was spiked into this subset as an internal standard. Straight chain alkanes with a single branch have been used as internal standards to track recovery of HBIs in other studies; they are commercially available and similar in structure to an HBI (Belt et al., 2014). Each spiked subset was dried

under nitrogen gas and redissolved in an equal volume of n-hexane. The hydrocarbon fraction of this total lipid extract was purified using open column chromatography. Samples were loaded dry onto a 0.5 g silica column (5 % deactivated, 100–200 mesh) and eluted with 4 mL (two column volumes) of n-hexane. These 4.4 mL extracts were concentrated to 200 μL and stored under argon at −20°C until GC–MS analysis.

The GC analysis was performed on a Thermo Scientific Trace 1310 Gas and a high temperature 30 m fused silica column (Agilent Technologies, DB-5HT, 0.25 mm i.d., 0.25 μm film). This was fed directly into a Thermo Scientific ISQ Single Quadrupole for MS analysis. We used a 1 μL injection of the hydrocarbon extract for analysis. The oven temperature was ramped (60°C-350°C; 5°C min^{-1}) followed by a temperature hold at 350°C for 30 min. The mass spectrometer transfer line temperature was 350°C, the ion source temperature was 275°C, and the ionization energy was 70 eV. We used an n-alkane standard (10–40 carbon, all even) to track retention time index of chromatographic peaks. A standard curve of 7-hexaoctadecane was used to calculate the limit of quantification for HBIs based on the prediction intervals as with other standard curves in this study (Popendorf et al., 2013).

2.7. Correlation network generation

In order to examine lipid species that cooccur with the ice cores, we performed a network correlation analysis using the peak area of retained lipid species annotations. Correlation network analysis is a data exploration technique used to find groups of correlated metabolites or 'clusters' that, in this case, likely derive from a similar microbial source. We used the 'R' package WGCNA to produce both a hard-threshold network for visualization as well as a soft-threshold (weighted) network that was used to define lipid clusters within the broader dataset (Langfelder and Horvath, 2008). Samples were rescaled setting the range for each to between 0 and 1. This reduced interfering effects of large biomass differences between samples. We used the Pearson's correlation coefficient between annotated lipid pairs to construct the network. To visualize the network with a hard threshold we retained pairs with a highly positive linear relationships ($r > 0.8$, $p < 0.01$) across rescaled ice core sample peak areas. To visualize, we additionally only considered species found in ≥ 95 % of ice core samples to ensure consistent correlations across sites. If a lipid pair met these criteria, they were linked in the resulting visualization. We additionally created a soft-threshold network to define clusters that included all lipid pairs, not just those that met the above critria. To do this, network correlation coefficients were raised to a power (weighted) to reduce noise but not hard cutoff of cluster connectivity was imposed. We used the "blockwiseModules" method from WGCNA define clusters, which resulted in 9 clusters across the dataset. Setting for this methods can be found in Table S2.

2.8. Sea ice caloric content calculations

We calculated the caloric content of sea ice by using the concentration of annotated lipids and estimating each lipid species heat of combustion. We estimated the heat of combustion based on the elemental composition of each lipid species using the following formula from Schmidt-Rohr (2015):

$$\Delta H^{\circ}c\ (kJ/mol) \approx -417*(C + 0.3H - 0.5O)$$

where $\Delta H^{\circ}c$ is the heat of combustion and *C, H,* and *O* are the number of each carbon, hydrogen, and oxygen atoms in the lipid molecule. This estimation relies on a set of assumptions about the frequency of bond types within organic molecules. However, for molecules with more carbon atoms than nitrogen and oxygen (of which all annotated lipids were) there was very low deviation between measured and predicted $\Delta H^{\circ}c$ (Schmidt-Rohr, 2015). We further validated the use of this estimate by comparing predicted values of ΔH°c with measured values of TAGs found in the literature (Freedman and Bagby, 1989; Krisnangkura, 1991). We found very high correspondence between predicted and measured ΔH°c ($R^2 = 0.99$, RMSE = 673 kJ mol^{-1}) as seen in Fig. S2. We are therefore confident that any error resulting from this estimation was well within the error of our ice core site replicates (Table 1). We calculated the caloric content and lipid inventories per m^2 of ice at each site by integrating the profiles of each lipid class over depth. (Table 1; Fig. 2).

3. Results

3.1. Lipid annotation results

Initial screening of mass spectra by our pipeline returned 158,546 peak groups and 12,440 annotations of possible intact lipid species. After validation of these annotations, via multiple criteria we retained a total of 1,173 intact lipid species present across all lipid classes which represented 68 % of the datasets total peak area. These lipids species were divided across 14 lipid classes in total; nine IPL membrane lipid classes (DGTS, DGTA, DGCC, SQDG, MGDG, DGDG, PG, PE, and PC), two neutral lipid classes (TAG, FAHFA-TAG), and three groups of pigments (Chlorophylls, Xanthophylls, and Carotenes). DGTS and DGTA lipid species were not separable from each other, and annotated lipids could contain representatives from both classes. See Table S4 for a list of lipid class abbreviations.

3.2. Chl a

Vertical lipid distributions in all ice cores were highly variable even within core sites pointing to large heterogeneity of the seasonal pack ice floes even on the scale of a few meters (Fig. 2). However, some consistent features were visible across sites. For example, Chl *a* concentrations tended to be low in the surface of ice cores and increase to a maximum between 25 and 50 cm in most cores before tapering off deeper in the core, a pattern that held true for most lipid species. Mean Chl *a* concentrations across the cores were 48 ± 52 μg/L while the maximum at most sites was much higher; concentrations exceeded 150 μg/L in at least one core at all but site 2 (Fig. 2A). Vertical integrations of Chl *a* were similarly variable with a mean of 9.6 ± 6.6 mg m^{-2} across all cores and a value maximum of 23 mg m^{-2} (Fig. 2B). We additionally quantified pheophytin *a* within our samples which was linearly correlated with Chl *a* in the sea ice ($R^2 = 0.63$, $p < 0.001$) though found in small amounts relative to Chl *a*. Pheophytin *a* was on average 10 ± 12 % of the Chl *a* mass in sea ice with this distribution highly skewed toward 0 %.

3.3. Triacylglycerols (TAGs) and Highly Branched Isoprenoids (HBIs)

TAGs were the most abundant single class of lipid we detected within the ice cores (Fig. 2C–D). Similar to other lipids, the mean concentrations were highly variable (249 ± 386 μg/L) with site 5 containing up to 2.6 mg/L. Mean vertically integrated TAG content was highest at sites 1, 3, and 5 and lowest at site 6. We detected a total of 389 unique TAG species ranging from 1 to 17 unsaturations per molecule and 32–73 fatty acid carbon atoms. However, the top five most abundant TAG species had a smaller range with only 2–7 unsaturations per molecule and 48–52 fatty acid carbon atoms (Table 3).

We were unable to detect any HBIs in the sample at each site with the highest Chl *a* level. We calculated our limit of detection in sea ice as 0.18 ± 0.1 μg/L using a 7-hexaoctadecane standard curve, internal standard, and volume of melted sea ice. If HBIs are present, they must be at least an order of magnitude lower than the lowest values of our total TAG and Chl *a* abundances.

3.4. Intact polar lipids

Overall concentrations and integrated amounts of total IPLs was comparable to TAGs at most sites (Fig. 2E–F). For phospholipids, we

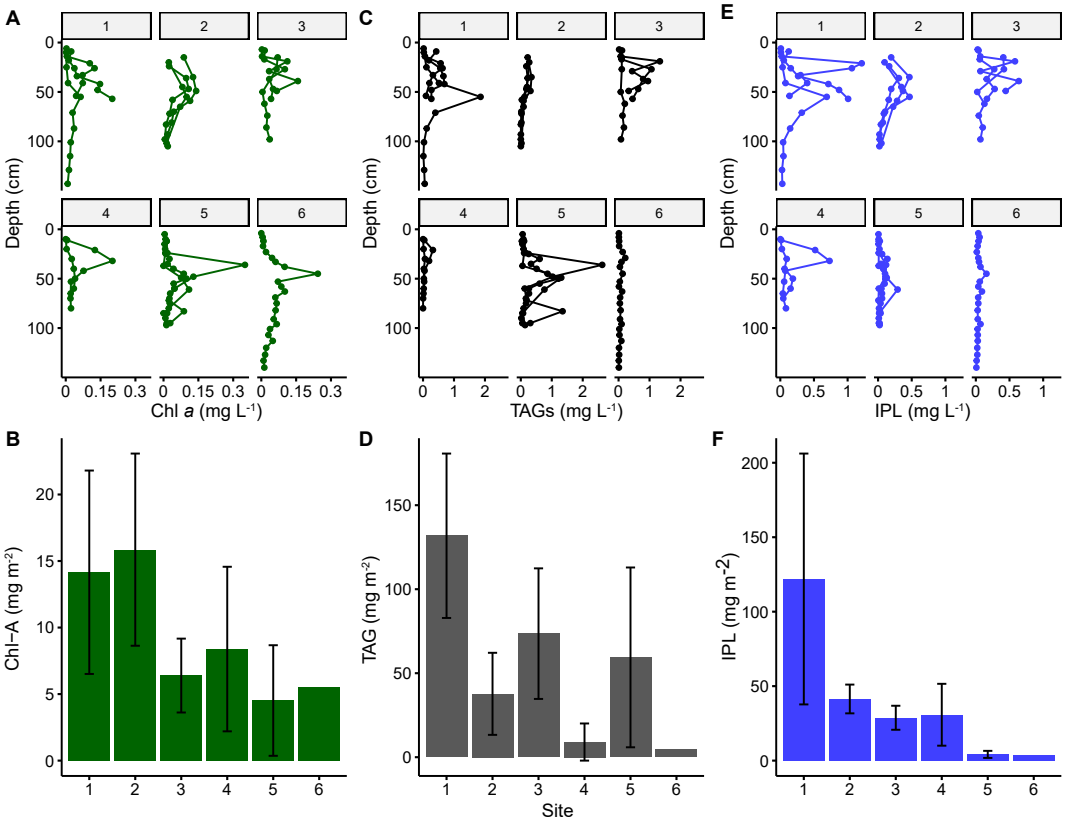

Fig. 2. Concentrations of Chl *a*, TAGs, and combined IPLs, in seasonal ice cores. Profiles within ice cores are shown for sites 1–6 as indicated with grey boxes inside panels A, C, and E. Vertical integration of ice cores for each lipid group is shown in panels B, D, and F. Depth values for samples are plotted at the bottom of each ice segment. Color indicates lipid class, Chl *a* (green) is shown in A and B, TAGs (grey) are shown in C and D, combined IPLs (blue) are shown in E and F.

Table 3
Dominant species across all ice core sites. The top five lipid species by mean concentration across all samples are listed for each class. Parenthesis shows the percentage of other lipid species in the same class that had a significant difference in concentration from that species (Pairwise Wilcox test, $p < 0.01$).

Lipid class	Top Five Species by Mean Concentration
DGTS/DGTA	DGTS/DGTA 42:11 (100 %), DGTS/DGTA 40:10 (100 %), DGTS/DGTA:34:5 (91 %), DGTS/DGTA 36:5 (44 %), DGTS/DGTA 44:12 (0 %)
DGCC	DGCC 36:6 (96 %), DGCC 38:6 (100 %), DGCC:44:12 (96 %), DGCC:40:11 (66 %), DGCC:46:8 (0 %)
DGDG	DGDG 36:7 (98 %), DGDG 36:10 (98 %), DGDG 36:9 (100 %), DGDG 32:2 (17 %), DGDG 34:7 (0 %)
MGDG	MGDG 36:9 (100 %), MGDG 36:10 (100 %), MGDG 32:7 (97 %), MGDG 32:8 (98 %), MGDG 32:6 (97 %)
SQDG	SQDG 32:4 (100 %), SQDG 34:5 (98 %), SQDG 38:9 (100 %), SQDG 32:1 (96 %), SQDG 36:5 (60 %)
PG	PG 36:6 (98 %), PG 32:1 (100 %), PG 32:2 (96 %), PG 30:1 (80 %), PG 34:2 (78 %)
PC	PC 36:6 (100), PC 40:10 (100), PC 42:11 (97), PC 40:11 (96), PC 38:6 (96)
PE	PE 32:2 (99 %), PE 32:1 (100), PE 38:6 (97 %), PE 30:1 (98 %), PE 42:11 (99 %)
TAG	TAG 48:2 (99 %), TAG 52:6 (99 %), TAG 48:3 (99 %), TAG 52:7 (99 %), TAG 50:2 (97 %)

detected multiple species of phosphatidylcholine (PC), phosphatidylethanolamine (PE), and phosphatidylglycerol (PG) within ice cores at every site. Abundance of phospholipids tracked total IPL levels consistently across sites. The relative abundance of PC was consistently high at sites 1–4 (21 ± 8.4 % of IPLs, Fig. S3). While site 5 had more variable quantities, at fast-ice site 6 the relative abundance of PC was quite low (10.5 ± 2.8 % of IPLs). The relative amount of PE was elevated at site 6 relative to the pack ice samples; site 6 had a mean of 55 ± 18 % PE compared to 13 ± 13 % for sites 1–5 (Fig. S3). PE species with 0–2 total unsaturations (≤1 per fatty acid) made up 85 ± 14 % of PE lipids at Site 6 which was also elevated in these low unsaturation PEs compared to others sites (Kruskal-Wallis test, $p < 0.001$). The dominant PC species were all unsaturated while the dominant PG and PE species contained a mix of polyunsaturated and monounsaturated species possibly pointing to separate pools for these lipid classes (Table 3).

We detected very low concentrations of betaine lipids relative to the abundances of other membrane lipids at all six sites (1.4 ± 2.6 μg/L DGTS/DGTA, 0.79 ± 1.6 μg/L DGCC, Fig. S3). The mean betaine lipid to PC ratio was 0.078 ± 0.09 with no sample above a 1:1 ratio. These values are in accordance with a highly nutrient replete pore-water of sea ice cores and best matched by values observed in P-replete diatom cultures (Van Mooy et al., 2009; Hunter et al., 2018). Overall, the most abundant betaine lipids had similar unsaturation levels to PC (Table 3). DGTS/DGTA was elevated relative to other replicates in three cores at sites 1, 3, and 4 above 50 cm depth. While the betaine lipid to PC ratio was indicative of replete conditions everywhere, these few hot spots, especially in a site 1 core where DGTS/DGTA reached close to 25 % of IPLs, may indicate patches of phosphate stress within the core where dissolved phosphate was drawn down (Fig. S3).

Photosynthetic glycolipids of the classes monogalactosyl diacylglycerol (MGDG), sulfoquinovosyl diacylglycerol (SQDG), and digalactosyl diacylglycerol (DGDG) were detected throughout the entirety of most ice cores. Collectively, they made up >50 % of the IPL mass in the majority of ice core samples; mean concentrations were 46 ± 76 μg/L MGDG, 17 ± 27 μg/L DGDG, and 30 ± 51 μg/L for SQDG. Similar to other IPLs, the dominant species were mostly polyunsaturated (Table 3). SQDG/PG ratios were very low (2.0 ± 1.4) indicating an environment with little phosphorus stress (Van Mooy et al., 2009), consistent with the

low betaine to PC ratio. Overall, glycolipids made up close to half of the IPLs in most samples (50 ± 21 %, Fig. S3) with no strong differences between the sites other than the top and bottom of site 6. As with phospholipids, glycolipid concentrations tended to track overall IPL levels.

3.5. Identification of FAHFA-TAGs

Multiple peak groups in the ice core samples were annotated as large TAGs (>60 fatty acid carbons) with two additional oxygen atoms (i.e., $C_nH_nO_8$). Initial inspection of these peaks MS/MS fragmentation spectra did not reveal fragments consistent with a peroxidized fatty acid but did however show diacylglycerol fragments consistent with a TAG structure. Due to this, we hypothesized that these TAGs could contain a fatty acid hydroxy fatty acid (FAHFA) moiety which would explain both their size as well as their additional oxygens. We reanalyzed three ice core samples with high concentrations of these TAGs (see Methods 2.4) along with a 1-Palmitoyl-2-12-PAHSA-3-Oleoyl-sn-glycerol (a FAHFA-TAG standard) to compare diagnostic MS/MS spectra.

At higher collision energies the FAHFA-TAG standard yielded diglyceride fragments consistent with the loss of two C16:0 fatty acids from the intact lipid structure as well as a fragment showing the loss of C18:1 and C16:0 fatty acid (Fig. S4A). Notably, the loss of the hydroxy fatty acid appeared to create a double bond on the diglyceride fragment which was apparent in the mass of both ions (Fig. S4, 577 and 603 ions). Additionally, lone C16:0 and C18:0 fatty acid fragments were observed at this collision energy (239 and 265 ions). Lower collision energies showed the diacylglyceride fragments where two fatty acids were lost but also revealed triacylgylceride fragments consistent with the loss of only one fatty acid: either the C16:0 hydroxy fatty acid or the C18:1 fatty acid (Fig. S4B). This is consistent with fragmentation patterns observed by other studies of FAHFA-TAGs (Tan et al., 2019; Paluchova et al., 2020).

We identified a prominent peak group within the ice core samples that followed a similar fragmentation pattern as the FAHFA-TAG standard with the added complexity that it appeared to be a mixture of multiple isomeric, and possibly regio-isomeric, FAHFA-TAGs (Fig. 3). Despite this added complexity we were able to observe both TAG fragments (803 and 777 ions) and diacylglyceride fragments (521, 549, and 575 ions) that were consistent with fragmentation of a mix of 16:0,14:0,18:1,16:0-TAG and 14:0,14:0,16:1,18:0-TAG isomers. Previous studies have reported variable intensities in fragments depending on the location of the FAHFA moiety in the TAG structure (Tan et al., 2019). However, given both the complex isomeric mixtures present and only a single standard for comparison we were not able to determine the carbon position of the hydroxyl group within the FAHFA structure.

Based on the retention time patterning around our MS/MS verified FAHFA-TAGs, we selected 33 other annotated FAHFA-TAG species that fit a series of peaks. Despite the detection of species across core sites, the concentration of candidate FAHFA-TAG species was comparatively low and mainly quantifiable at site 1. The maximum FAHFA-TAG concentration detected was 39 μg/L which coincided with an approximately 50x larger TAG peak (1857 μg/L TAG) at 55 cm in core 1C. Where FAHFA-TAGs were quantifiable, they made up 0.7 ± 0.5 % of the total TAG pool (i.e. TAG + FAHFA-TAG) with a maximum abundance (2 %) in the aforementioned 55 cm sample (Fig. S5).

3.6. Sea ice caloric content

Heat of combustion for each lipid species scaled with carbon content. Overall, IPLs had a heat of combustion ranging from 28.09 to 37.48 kJ g^{-1} while TAGs ranged from 36.78 to 41.44 kJ g^{-1}; an energy boost deriving from the addition of an extra fatty acid and overall lower C:O ratio than most IPLs (Fig. 4). The heat of combustion for detected FAHFA-TAGs overlapped with the TAG range (36.79–40.16 kJ g^{-1}) as an additional fatty acid added more carbon but also two more oxygen atoms. Despite a two-fold difference in heat of combustion across detectable lipid species, overall caloric content of the cores was driven much more by the multiple order of magnitude difference in species concentrations observed within the ice (Fig. 4). As such, despite their high energy density, FAHFA-TAGs contributed negligibly to caloric content within the ice due to their low concentrations.

The caloric content of individual cores ranged between 0.48 kJ m^{-2} at site 6 and 12.43 kJ m^{-2} in a single core at site 1. However, among pack ice sites 1–5, a Kruskal-Wallis test showed no site was significantly different in its median caloric content ($p = 0.206$). Given the low number of replicates at each site ($n = 3$) this result should be treated with caution. However, it would appear that the kilometer scale variability of caloric content between sites may not be greater than the 1–10 m scale variability between ice cores at a single site. Thus, the mean of all pack ice sites (4.45 ± 3.47 kJ m^{-2}) is most useful when considering caloric content of pack ice in the region.

3.7. Class level correlations and species level correlation network analysis

Interestingly, while TAGs displayed a mid-depth maximum in some cores similar to Chl *a*, the overall correlation between TAG and Chl *a* levels was fairly weak (Fig. 5A). While making up a large fraction of the lipid mass, total TAG concentrations were only weakly correlated with Chl *a* in pack ($R^2 = 0.45$, $p < 0.001$) and fast ice ($R^2 = 0.26$, $p = 0.007$, Fig. 5A). We assessed the possibility that Chl *a* degradation into pheophytin *a* during melting may have contributed to low correlations between TAG and Chl *a* content but found that it could not explain the error in this regression (Fig. S6). Correlations between Chl *a* + pheophytin *a* versus TAG content shifted minimally and were less correlated than Chl *a* versus TAG content. Thus, while melting conditions may have converted some Chl *a* into pheophytin *a* it does not appear to have affected the overall relationship between the variables. Total lipid caloric content and Chl *a* were more closely correlated than TAG content and Chl *a* levels, but again highlighted large disparities between pack and fast ice (Fig. 5B). Despite better correlations, fast ice had a lower calorie to Chl *a* relationship (1.78 J ug^{-1} Chl *a*) than pack ice (3.25 J ug^{-1} Chl *a*) raising questions about the utility of Chl *a* in predicting sea ice caloric content.

To examine correlations between these individual lipid species within the ice cores and gain insights into covariance patterns that may indicate source we used a correlation network analysis. Correlation network analysis yielded nine clusters, six of which were particularly prominent in our network visualization (Fig. S7, Fig. S8). Only 18 % of lipid species were not placed in a cluster by the WGCNA methods. The most correlated lipids from clusters “A”, “B”, and “C” contained almost entirely TAGs separated by different levels of unsaturation; clusters “A” and “B” contained more highly unsaturated TAG species than cluster “C”. FAHFA-TAGs also formed a tight group within clusters ‘A” and “I”. IPLs were well distributed but 61 % of species grouped into four clusters “D”, “E”, “F”, and “H”. The “D” and “H” clusters contained a wide mix of glycolipids, PC, and betaine lipid species.

Clusters of IPLs appeared to separate by taxonomic source in the network. The two IPL clusters “E” and “F” contained more PE species and are indicative of the lipid composition of heterotrophic bacteria (Popendorf et al., 2011; Sebastián et al., 2016). The other two clusters of diverse IPLs (“D” and “H”) could be interpreted as a broad photosynthetic microbial signal; lipids in this cluster contain polyunsaturated glycolipids often found in eukaryotic algae along with PC lipids which dominate eukaryotic membranes (Hunter et al., 2018). Based on the above interpretation, we were curious to see what distributions of these IPL clusters looked like within the ice cores profiles as a rough tracker of relative bacteria and algal abundance (Fig. S9). The bacterial clusters (E+F) were generally low as a percentage of total lipids (3.5 % ± 5.3 %) and low compared to the algal clusters. However, at site 6, bacterial IPLs clusters (E+F) had a large spike in the ice surface that reached almost 40 % of total lipids and showed levels around ~20 % of total lipids in the

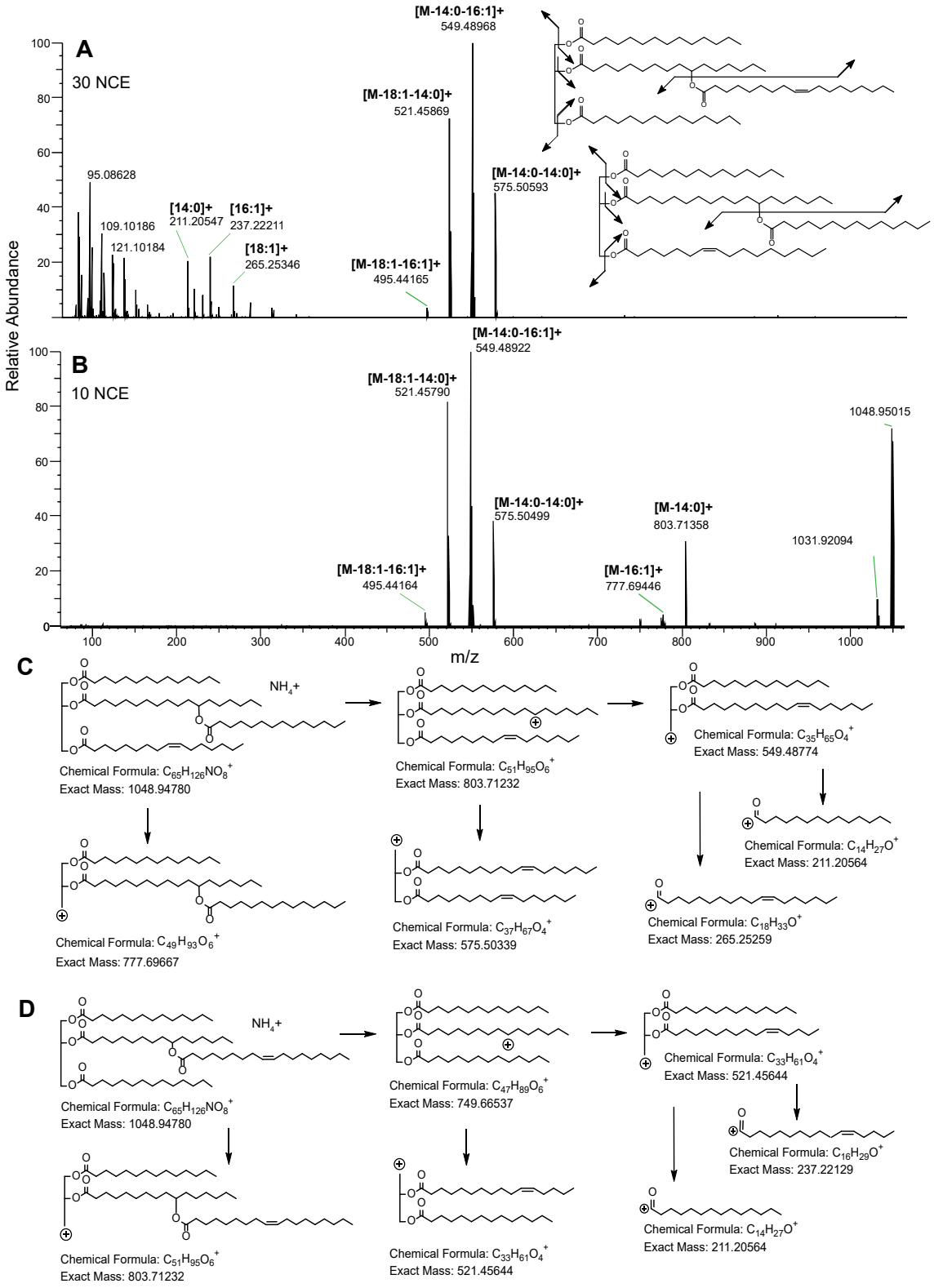

Fig. 3. FAHFA-TAG fragmentation spectra and possible structure. MS/MS fragmentation spectra is shown for an annotated FAHFA-TAG compound from sea ice cores under two collision energies: HCD 30 in A and HDC 10 in B. Chromatographic peak contained a mixture of two isomeric compounds shown in top right of panel A with fragmentation locations on the structure. Losses of fatty acids from precursor ion are show above prominent fragments. Fragmentation pathways for both FAHFA-TAG isomers are shown in panels C and D respectively. Note that positions of fatty acids on glycerol backbone as well as position of the fatty acid hydroxyl moiety within the proposed structure (attachment drawn at carbon number 12) are not determinable from this MS/MS spectra and could be variable.

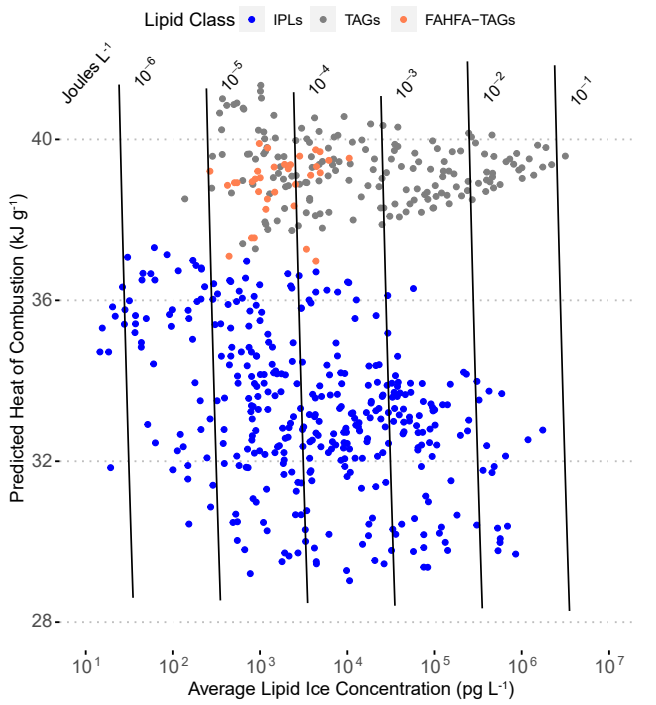

Fig. 4. Predicted heat of combustion verse mean concentration in sea ice for TAGs, FAHFA-TAGs, and IPLs. Average lipid concentrations (pg L^{-1}) within ice cores for each quantifiable lipid species is shown on the x-axis. Estimated heat of combustion for each lipid species (kJ g^{-1}) is shown on the y-axis. Lines of constant energy (Joules L^{-1}) are drawn in black with their values printed at the top right of the line. Point color indicates lipid class.

bottom of the same core (Fig. S9).

4. Discussion

4.1. Lipid abundance and distribution in sea ice

Unlike primary production in other part of the ocean, sea ice based growth is not accessible to remote sensing and must inherently rely on in situ measurements for understanding of the underlying geochemistry. Measurements constraining the variability in carbon composition within seasonal ice are thus important to understand the underlying geochemistry of these communities. We found lipid content within the sea ice was variably distributed even within sites where cores were sampled 5–10 m from each other. Formation of pack ice in the fall can create heterogenous internal structure which in turn creates variable internal environmental conditions for ice microbes (Garrison, 1991). Additionally, inconsistent melting of the ice during the spring creates further heterogeneity. While small scale spatial heterogeneity is a known feature of sea ice ecosystems, studies interested in chemical compositions within sea ice would be served by a high number of replicates to gain perspective on mean conditions (van Leeuwe et al., 2018). Our measurements of integrated Chl *a* levels in pack ice are near or just above the November mean values for pack ice from larger pan-Antarctic datasets (~5 mg m^{-2}, Meiners et al., 2012). Both maximum concentrations and vertically integrated inventories of Chl *a* were in the range of reported values for internal pack ice during the spring in the Weddell sea and Ross Sea (1–29 mg m^{-2}, Arrigo, 2017). However, these values are much lower than Chl *a* concentrations observed in the bottom and platelet zones of Antarctica sea ice (76–1090 mg m^{-2}, Arrigo, 2017). Phytoplankton can form dense communities in the platelet bottom of sea ice, however these communities were absent at the sites we sampled likely due to melting before we arrived. The lack of HBIs in our samples may also be due to the lack of this ice bottom layer before our arrival.

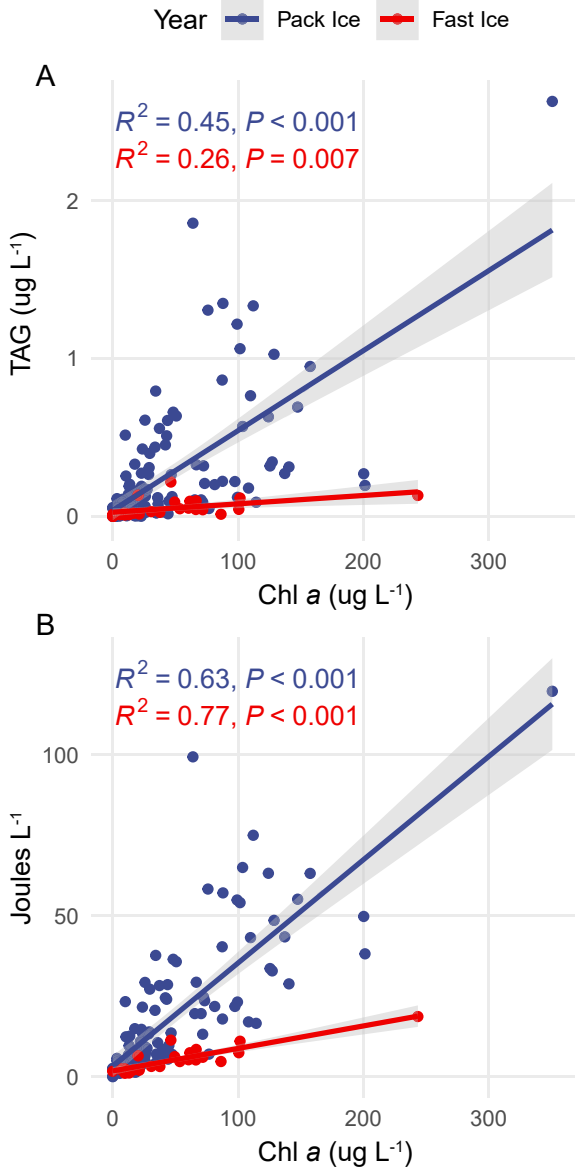

Fig. 5. Chlorophyll *a* versus sea ice lipid caloric content in pack ice and fast ice. Correlations between lipid concentrations in ice cores are shown for (A) TAG verse Chl *a* and (B) total caloric content versus Chl *a*. Linear fits are shown for pack (blue) and fast (red) ice types.

Previous work has identified the diatom *Berkeleya adeliensis* as a possible source for the sea ice proxy HBI $IPSO_{25}$ (Belt et al., 2016). Since this diatom seems to be associated with the bottom ice community where it is detected, it seems likely that HBIs are particularly rich in bottom layers of sea ice and were lost before our sampling.

Network analysis and lipid class distributions pointed to complex microbial separation within ice. While lipid concentrations were variable between sites, the relative abundance of lipid classes were more consistent with the exception of the single fast ice site (Site 6). This site showed comparable levels of Chl *a* to other sites, while having less IPLs and TAGs (Fig. 2). Land fast sea ice has a distinct structure and origin from pack ice that is known to lead to a different vertical structure and internal community (van Leeuwe et al., 2018). While the upper portion of pack ice is known to be a region of high biomass, blooms within the upper third of fast ice are rarer and usually timed with winter/spring conditions when observed (Meiners et al., 2018). The higher relative abundance of low unsaturation PE lipids could point to a greater fraction of bacteria relative to other sites as PE is usually the dominant

phospholipid in bacterial membranes under replete conditions (Carini et al., 2015; Sebastián et al., 2016). This was recapitulated by network analysis that highlighted the top zone of site 6 as being more bacteria dominated than other core (Fig. S8). While further work is needed to directly link these lipid abundances to cell densities, our geochemical analysis indicates there may be distinct microbial zonation within ice under certain conditions.

Separation of lipid species by taxonomic source in network analysis is logical, but we additionally see that lipids with broadly different biochemical roles (i.e. energy storage lipids, membrane lipids, and pigments) were separable from each other by their correlations. Cells deeper in the ice are likely to photoacclimate and need more Chl *a* per cell to support similar levels of production as communities nearer to the surface (van Leeuwe et al., 2018). On top of this, TAGs serve a specific cellular role in energy storage and can increase in phytoplankton in response to many types of environmental stressors, possibly decoupling their abundance from other lipid groups (Hu et al., 2008). We hypothesize that these different biochemical roles for Chl *a* and TAG resulted in the variable ratios between them in the sea ice as well as their separation in network analysis (Fig. S9). While we detected pheophytin *a* within the ice, it's abundance did not explain the error in Chl *a* verse TAG correlations (Fig. S6). As with other studies that have shown a variable Chl *a* to particulate organic carbon ratio in sea ice, our work further illustrates that Chl *a* levels alone are ineffective at predicting the carbon content of sea ice likely due to photoacclimation (Arrigo, 2003).

4.2. Sea ice lipids represent a calorically valuable resource for zooplankton

A combination of biomass levels and physical protection make sea ice, and its lipid stores, a valuable resource to higher trophic levels. Comparisons with water columns from Arctic and Antarctic regions showed that the depth integrated lipid fraction of sea ice in our study is comparable to the total caloric content per square meter of some polar water columns (Choe et al., 2021 and citations there in). This was driven by a dense region of sea ice biomass between 25 and 50 cm where mean lipid caloric content was 31 ± 22 kJ m^{-3} with a maximum of 119 kJ m^{-3} compared to a range of 2.5–15 kJ m^{-3} for polar water columns from various seasons (Choe et al., 2021). The accessibility of these lipid stores to zooplankton grazers present in and around melting sea ice is hard to estimate directly. Large microzooplankton grazers that cannot fit within brine channels must feed on the sea ice surface; however, rapid spring melting of pack ice may ultimately expose most of the internal particulate contents of pack ice to the water column. A portion of this biomass is likely contained in microbes too small to graze by large zooplankton. There are few studies on the consumption of microbes other than algae from sea ice, but our results imply that the majority of the lipid stores are unlikely to be derived from bacteria (Fig. S9). While stores of lipids and other molecules have been quantified within sea ice, the caloric content specifically of such stores is not always quantified (Duncan and Petrou, 2022). Our approach here, directly estimating the caloric content of quantified lipids, puts our geochemical measurements in the biological context of Antarctic food webs.

Zooplankton feeding on sea ice as it melts directly link this within-ice carbon stock both with benthic communities (via fecal pellets) and large food webs. A large range of Antarctic consumers rely on sustenance from sea ice micro-organisms; a study by Jia et al., 2016 revealed that copepods from the genus *Oithona*, pteropods (*Limacina helicina*), and other Antarctic crustacean grazers have isotope values indicating high feeding on sea ice. The reliance of these specific groups on sea ice lipid stores is yet to be fully explored. Of particular note in the Antarctic ecosystem, both due to its reliance on sea ice and shear abundance, is *E. superba*. These krill feed directly on dense surface patches of internal pack ice phytoplankton which has been well characterized and was directly observed during ice sampling in this study as well (Stretch et al., 1988). *E. superba*, and their fecal pellets, additionally represent the major control on carbon export in north regions of the WAP. A recent study from Trinh et al., 2023 utilized 20 years of data to illustrate the connection between krill life cycle and carbon export. Studies using fatty acid isotopes suggest that a high proportion (88 %) of lipids in overwintering pre-adult krill derived from sea ice algae further emphasizing a direct trophic link to our caloric measurements (Kohlbach et al., 2017). Rapid regional warming and sea ice retreat along the WAP has pushed *E. superba* distributions southward since the 1970s and possibly lowered the survival of juvenile krill (Atkinson et al., 2019). Better data on the carbon contents of sea ice should increase our understanding of population constraints for this keystone species.

4.3. FAHFA-TAGs as possible products of oxidative stress in phytoplankton

While FAHFA moieties have been found in plants, fungi, and animals their biochemical roles have not been completely discerned (Zhang et al., 2012; Brejchova et al., 2020). A variety of structurally related FAHFA-TAG compounds containing one or multiple additional fatty acids (also called "TAG estolides") are known from plant oils (e.g. *Lesqueralla auriculata*) and appear somewhat widely distributed among plants (Hayes et al., 1995; Isbell, 2011; Liberati-Čizmek et al., 2019). Recently, Fais et al. (2021) detected free FAHFAs in *C. melkonianii,* an extremophile cryptophyte from a mining run-off site highly polluted by heavy metals and sulfate. Despite robust research on plants, FAHFA moieties have not been reported widely in phytoplankton.

Brejchova et al., 2020 have reviewed a growing understanding that FAHFA-TAGs play a role as downstream products in removal of oxidized membrane lipids from cell membranes. In brief, the pathway proposed is as follows: a membrane lipid is oxidized, the resulting hydroxy fatty acid is cleaved and coupled with an acyltransferase to create a FAHFA, and finally the resulting FAHFA is incorporated into a FAHFA-TAG for storage. While not necessarily related to oxidative stress, pathways for the creation of hydroxy fatty acids and the shuttling of them to TAGs is known in plants (Chen et al., 2011). Formation of hydroxyl fatty acids on PUFA in marine diatoms is well characterized via lipoxygenase enzymes in response to grazing stress (Fontana et al., 2007). Additionally, abiotic oxidation of cell membranes from UV light may be an alternative pathway for hydroxyl fatty acid formation in the Antarctic (Collins et al., 2018). While the exact enzymes for forming FAHFAs from hydroxyl fatty acid precursors are not known, some eukaryotic cells do carry out this process (Kuda et al., 2018; Rodríguez et al., 2019).

Based on these known biosynthetic pathways and the ice core environment being one of high oxidative stress, we speculate that FAHFA-TAGs are formed from oxidized membrane lipid fatty acids as described above. Surface ice core brines in the summer represent areas of high light conditions and very high dissolved nitrate ions creating conditions for oxidative stress (King et al., 2005). While our initial screening of ice core lipids did not reveal high levels of intact oxylipins, FAHFA-TAGs could represent a much more stable and long-lived reservoir in which to store these possibly deleterious oxidation products. The saturation state of these compounds may point to formation mechanism; some of the more abundant FAHFA-TAG species only have 2–3 unsaturations on the total molecule. Rates of abiotic photoxidation are likely highest in lipid fatty acids with more unsaturations (5+), therefor the dominance of lower unsaturation FAHFA-TAG species implies enzymatic origin. PUFA hydroxy fatty acids are known precursors to unsaturated aldehydes able to spur cell death pathways in diatoms (Leflaive and Ten-Hage, 2009). Shuttling membrane hydroxy fatty acids toward FAHFA-TAGs rather than into other breakdown products could both preserve membrane integrity and delay unwanted stress pathways (Bhattacharjee, 2014). Further work will be needed to characterize the exact structure and source of FAHFA-TAGs within this environment. If FAHFA-TAGs are indeed formed from the oxidation of membrane lipid fatty acids, they may additionally serve as faithful recorders of different oxidative pathways due to the regiospecificity of oxidation effects

(Rontani et al., 2011, 2012).

5. Conclusions

Untargeted screening of sea ice lipid cores revealed a spatially variable microbial community with sections of high lipid biomass. We found Chl *a* concentrations within the sea ice were in the range of previous observations of Antarctic pack ice but were a poor predictors of overall lipid levels. We found that TAG and IPLs contributed around equally to the detectable caloric content within the ice cores. IPL ratios between lipid classes were more uniform with a notable lack of betaine lipids when compared to marine water columns, a finding consistent with a replete nutrient environment for microbes. Measures of lipid energy stores showed high lipid caloric concentrations, especially in the upper half of ice cores, reinforcing the value of sea ice habitats for trophic consumers during the spring melt. We detected multiple species of FAHFA-TAGs alongside TAGs that may be the result of oxidative stress within phytoplankton. These results encourage a full accounting of the macromolecular distributions of labile material within polar sea ice for a detailed understanding of biochemical processes at play in a rapidly changing ecosystem.

Data availability

Data are available through Mendeley Data at https://doi.org/10.17632/rn43h5g585.1.

Declaration of competing interest

The authors declare that they have no known competing financial interests or personal relationships that could have appeared to influence the work reported in this paper.

Acknowledgements

We would like to thank the captain, crew, and ASC staff of the RV *Lawrence M. Gould* for their work during cruise LMG1810 that facilitated the collection of these samples as well as the 2018 science staff of Palmer station that provided logistical support before and after the cruise. Additionally, we would like to acknowledge K. Perry and M. Small for their lab work preparing some of these lipid samples. We would additionally like to thank three anonymous reviewers for their detailed and constructive reviews. This research was supported by grants to B.A.S.V. M, from National Science Foundation (OPP-1543328, OPP-2026045, OCE-1756254, and OCE-2022597) the Marine Microbiology Initiative division of the Gordon and Betty Moore Foundation (5073), and the Simons Foundation (721229).

Appendix A. Supplementary material

Supplementary materials includes a single file containing Tables S1–S4 and Figs. S1-S9. This includes tables with site locations as well as information on lipid standards used. Figures include results of TAG response model, validation of caloric value estimates, compositional bar plots of IPLs, network visualizations, and fragmentation spectra of FAHFA-TAG standard. Supplementary material to this article can be found online at https://doi.org/10.1016/j.gca.2024.01.003.

References

Arrigo, K.R., 2014. Sea ice ecosystems. Annu. Rev. Mar. Sci. 6, 439–467.
Arrigo, K.R., 2017. In: Sea ice as a habitat for primary producers. In Sea Ice John Wiley & Sons Ltd, pp. 352–369.
Atkinson, A., Hill, S.L., Pakhomov, E.A., Siegel, V., Reiss, C.S., Loeb, V.J., Steinberg, D.K., Schmidt, K., Tarling, G.A., Gerrish, L., Sailley, S.F., 2019. Krill (Euphausia superba) distribution contracts southward during rapid regional warming. Nat. Clim. Change 9, 142–147.
Becker, K.W., Collins, J.R., Durham, B.P., Groussman, R.D., White, A.E., Fredricks, H.F., Ossolinski, J.E., Repeta, D.J., Carini, P., Armbrust, E.V., Van Mooy, B.A.S., 2018. Daily changes in phytoplankton lipidomes reveal mechanisms of energy storage in the open ocean. Nat. Commun. 9, 5179.
Belt, S.T., Brown, T.A., Ampel, L., Cabedo-Sanz, P., Fahl, K., Kocis, J.J., Massé, G., Navarro-Rodriguez, A., Ruan, J., Xu, Y., 2014. An inter-laboratory investigation of the Arctic sea ice biomarker proxy IP25 in marine sediments: key outcomes and recommendations. Clim. Past 10, 155–166.
Belt, S.T., Smik, L., Brown, T.A., Kim, J.-H., Rowland, S.J., Allen, C.S., Gal, J.-K., Shin, K.-H., Lee, J.I., Taylor, K.W.R., 2016. Source identification and distribution reveals the potential of the geochemical Antarctic sea ice proxy IPSO25. Nat. Commun. 7, 12655.
Benton, H.P., Wong, D.M., Trauger, S.A., Siuzdak, G., 2008. XCMS^2: processing tandem mass spectrometry data for metabolite identification and structural characterization. Anal. Chem. 80, 6382–6389.
Bernaerts, T.M.M., Gheysen, L., Foubert, I., Hendrickx, M.E., Van Loey, A.M., 2019. The potential of microalgae and their biopolymers as structuring ingredients in food: a review. Biotechnol. Adv. 37, 107419.
Bhattacharjee, S., 2014. Membrane lipid peroxidation and its conflict of interest: the two faces of oxidative stress. Curr. Sci. 107, 1811–1823.
Bowman, J.S., Van Mooy, B.A.S., Lowenstein, D.P., Fredricks, H.F., Hansel, C.M., Gast, R., Collins, J.R., Couto, N., Ducklow, H.W., 2021. Whole community metatranscriptomes and lipidomes reveal diverse responses among Antarctic phytoplankton to changing ice conditions. Front. Mar. Sci. 8, 593566.
Brejchova, K., Balas, L., Palůchová, V., Brezinova, M., Durand, T., Kuda, O., 2020. Understanding FAHFAs: from structure to metabolic regulation. Prog. Lipid Res. 79, 101053.
Carini, P., Van Mooy, B.A.S., Thrash, J.C., White, A., Zhao, Y., Campbell, E.O., Fredricks, H.F., Giovannoni, S.J., 2015. SAR11 lipid renovation in response to phosphate starvation. Proc. Natl. Acad. Sci. 112, 7767–7772.
Chen, G.Q., Lin, J.-T., Lu, C., 2011. Hydroxy fatty acid synthesis and lipid gene expression during seed development in Lesquerella fendleri. Ind. Crop. Prod. 34, 1286–1292.
Choe, K., Yun, M., Park, S., Yang, E., Jung, J., Kang, J., Jo, N., Jaehong, K., Jaesoon, K., Lee, S.H., 2021. Spatial patterns of macromolecular composition of phytoplankton in the Arctic Ocean. Water 13, 2495.
Collins, J.R., Edwards, B.R., Fredricks, H.F., Van Mooy, B.A.S., 2016. LOBSTAHS: an adduct-based lipidomics strategy for discovery and identification of oxidative stress biomarkers. Anal. Chem. 88, 7154–7162.
Collins, J.R., Fredricks, H.F., Bowman, J.S., Ward, C.P., Moreno, C., Longnecker, K., Marchetti, A., Hansel, C.M., Ducklow, H.W., Van Mooy, B.A.S., 2018. The molecular products and biogeochemical significance of lipid photooxidation in West Antarctic surface waters. Geochim. Cosmochim. Acta 232, 244–264.
Duncan, R.J., Petrou, K., 2022. Biomolecular composition of sea ice microalgae and its influence on marine biogeochemical cycling and carbon transfer through polar marine food webs. Geosciences 12, 38.
Fais, G., Malavasi, V., Scano, P., Soru, S., Caboni, P., Cao, G., 2021. Metabolomics and lipid profile analysis of Coccomyxa melkonianii SCCA 048. Extremophiles 25, 357–368.
Fontana, A., d'Ippolito, G., Cutignano, A., Romano, G., Lamari, N., Massa, G.A., Cimino, G., Miralto, A., Ianora, A., 2007. LOX-induced lipid peroxidation mechanism responsible for the detrimental effect of marine diatoms on Zooplankton grazers. Chembiochem 8, 1810–1818.
Foyer, C.H., 2018. Reactive oxygen species, oxidative signaling and the regulation of photosynthesis. Environ. Exp. Bot. 154, 134–142.
Freedman, B., Bagby, O., 1989. Heats of combustion of fatty esters and Triglycerides I. J. Am. Oil Chemists' Soc. 66, 5.
Garrison, D.L., 1991. Antarctic sea ice biota. Am. Zool. 31, 17–34.
Gleitz, M., vd Loeff, M.R., Thomas, D.N., Dieckmann, G.S., Millero, F.J., 1995. Comparison of summer and winter inorganic carbon, oxygen and nutrient concentrations in Antarctic sea ice brine. Mar. Chem. 51, 81–91.
Han, X., Gross, R.W., 2001. Quantitative analysis and molecular species fingerprinting of triacylglyceride molecular species directly from lipid extracts of biological samples by electrospray ionization tandem mass spectrometry. Anal. Biochem. 295, 88–100.
Hayes, D.G., Kleiman, R., Phillips, B.S., 1995. The triglyceride composition, structure, and presence of estolides in the oils of Lesquerella and related species. J. Am. Oil Chemists' Soc. 72, 559–569.
Holčapek, M., Lísa, M., Jandera, P., Kabátová, N., 2005. Quantitation of triacylglycerols in plant oils using HPLC with APCI-MS, evaporative light-scattering, and UV detection. J. Sep. Sci. 28, 1315–1333.
Holm, H.C., Fredricks, H.F., Bent, S.M., Lowenstein, D.P., Ossolinski, J.E., Becker, K.W., Johnson, W.M., Schrage, K., Mooy, B.A.S.V., 2022. Global ocean lipidomes show a universal relationship between temperature and lipid unsaturation. Science 376, 1487–1491.
Hu, Q., Sommerfeld, M., Jarvis, E., Ghirardi, M., Posewitz, M., Seibert, M., Darzins, A., 2008. Microalgal triacylglycerols as feedstocks for biofuel production: perspectives and advances. Plant J. 54, 621–639.
Hunter, J.E., Brandsma, J., Dymond, M.K., Koster, G., Moore, C.M., Postle, A.D., Mills, R. A., Stabb, A.G.S.E.V., 2018. Lipidomics of *Thalassiosira pseudonana* under phosphorus stress reveal underlying phospholipid substitution dynamics and novel diglycosylceramide. Appl. Environ. Microbiol. 84, e02034–e10117.
Isbell, T.A., 2011. Chemistry and physical properties of estolides. Grasas y Aceites 62, 8–20.
Ivanov, I., Heydeck, D., Hofheinz, K., Roffeis, J., O'Donnell, V.B., Kuhn, H., Walther, M., 2010. Molecular enzymology of lipoxygenases. Arch. Biochem. Biophys. 503, 161–174.

Jia, Z., Swadling, K.M., Meiners, K.M., Kawaguchi, S., Virtue, P., 2016. The zooplankton food web under East Antarctic pack ice – A stable isotope study. Deep Sea Res. Part II 131, 189–202.
King, M.D., France, J.L., Fisher, F.N., Beine, H.J., 2005. Measurement and modelling of UV radiation penetration and photolysis rates of nitrate and hydrogen peroxide in Antarctic sea ice: an estimate of the production rate of hydroxyl radicals in first-year sea ice. J. Photochem. Photobiol. A Chem. 176, 39–49.
Kohlbach, D., Lange, B.A., Schaafsma, F.L., David, C., Vortkamp, M., Graeve, M., van Franeker, J.A., Krumpen, T., Flores, H., 2017. Ice algae-produced carbon is critical for overwintering of Antarctic Krill Euphausia superba. Front. Mar. Sci. 4, 310.
Krisnangkura, K., 1991. Estimation of heat of combustion of triglycerides and fatty acid methyl esters. J. Am. Oil Chem. Soc. 68, 56–58.
Kuda, O., Brezinova, M., Silhavy, J., Landa, V., Zidek, V., Dodia, C., Kreuchwig, F., Vrbacky, M., Balas, L., Durand, T., Hübner, N., Fisher, A.B., Kopecky, J., Pravenec, M., 2018. Nrf2-mediated antioxidant defense and peroxiredoxin 6 are linked to biosynthesis of palmitic acid ester of 9-hydroxystearic acid. Diabetes 67, 1190–1199.
Kuhl, C., Tautenhahn, R., Böttcher, C., Larson, T.R., Neumann, S., 2012. CAMERA: an integrated strategy for compound spectra extraction and annotation of liquid chromatography/mass spectrometry data sets. Anal. Chem. 84, 283–289.
Kuosa, H., Kaartokallio, H., 2006. Experimental evidence on nutrient and substrate limitation of Baltic Sea sea-ice algae and bacteria. Hydrobiologia 554, 1–10.
Langfelder, P., Horvath, S., 2008. WGCNA: an R package for weighted correlation network analysis. BMC Bioinf. 9, 559.
Leflaive, J., Ten-Hage, L., 2009. Chemical interactions in diatoms: role of polyunsaturated aldehydes and precursors. New Phytol. 184, 794–805.
Liberati-Čizmek, A.-M., Biluš, M., Brkić, A.L., Barić, I.C., Bakula, M., Hozić, A., Cindrić, M., 2019. Analysis of fatty acid esters of hydroxyl fatty acid in selected plant food. Plant Foods Hum. Nutr. 74, 235–240.
Lizotte, M.P., 2001. The contributions of sea ice algae to Antarctic marine primary production. Am. Zool. 41, 57–73.
Meiners, K.M., Vancoppenolle, M., Thanassekos, S., Dieckmann, G.S., Thomas, D.N., Tison, J.-L., Arrigo, K.R., Garrison, D.L., McMinn, A., Lannuzel, D., van der Merwe, P., Swadling, K.M., Smith, W.O., Melnikov, I., Raymond, B., 2012. Chlorophyll *a* in Antarctic sea ice from historical ice core data: chlorophyll in antarctic sea ice. Geophys. Res. Lett. 39, L21602.
Meiners, K.M., Vancoppenolle, M., Carnat, G., Castellani, G., Delille, B., Delille, D., Dieckmann, G.S., Flores, H., Fripiat, F., Grotti, M., Lange, B.A., Lannuzel, D., Martin, A., McMinn, A., Nomura, D., Peeken, I., Rivaro, P., Ryan, K.G., Stefels, J., Swadling, K.M., Thomas, D.N., Tison, J.-L., van der Merwe, P., van Leeuwe, M.A., Weldrick, C., Yang, E.J., 2018. Chlorophyll-a in Antarctic Landfast Sea ice: A first synthesis of historical ice Core data. J. Geophys. Res. Oceans 123, 8444–8459.
Paluchova, V., Oseeva, M., Brezinova, M., Cajka, T., Bardova, K., Adamcova, K., Zacek, P., Brejchova, K., Balas, L., Chodounska, H., Kudova, E., Schreiber, R., Zechner, R., Durand, T., Rossmeisl, M., Abumrad, N.A., Kopecky, J., Kuda, O., 2020. Lipokine 5-PAHSA is regulated by adipose triglyceride lipase and primes adipocytes for de novo lipogenesis in mice. Diabetes 69, 300–312.
Popendorf, K.J., Lomas, M.W., Van Mooy, B.A.S., 2011. Microbial sources of intact polar diacylglycerolipids in the Western North Atlantic Ocean. Org Geochem. 42, 803–811.
Popendorf, K.J., Fredricks, H.F., Van Mooy, B.A.S., 2013. Molecular ion-independent quantification of polar glycerolipid classes in marine plankton using triple quadrupole MS. Lipids 48, 185–195.
Ralph, P.J., Ryan, K.G., Martin, A., Fenton, G., 2007. Melting out of sea ice causes greater photosynthetic stress in algae than freezing in1. J. Phycol. 43, 948–956.
Rodríguez, J.P., Guijas, C., Astudillo, A.M., Rubio, J.M., Balboa, M.A., Balsinde, J., 2019. Sequestration of 9-hydroxystearic acid in FAHFA (fatty acid esters of hydroxy fatty acids) as a protective mechanism for colon carcinoma cells to avoid apoptotic cell death. Cancers 11, 524.
Rontani, J.-F., Zabeti, N., Wakeham, S.G., 2011. Degradation of particulate organic matter in the equatorial Pacific Ocean: biotic or abiotic? Limnol. Oceanogr. 56, 333–349.
Rontani, J.-F., Charriere, B., Forest, A., Heussner, S., Vaultier, F., Petit, M., Delsaut, N., Fortier, L., Sempéré, R., 2012. Intense photooxidative degradation of planktonic and bacterial lipids in sinking particles collected with sediment traps across the Canadian Beaufort shelf (arctic Ocean). Biogeosciences 9, 4787–4802.
Rontani, J.-F., Amiraux, R., Lalande, C., Babin, M., Kim, H.-R., Belt, S.T., 2018. Use of palmitoleic acid and its oxidation products for monitoring the degradation of ice algae in Arctic waters and bottom sediments. Org Geochem. 124, 88–102.
Sackett, O., Petrou, K., Reedy, B., De Grazia, A., Hill, R., Doblin, M., Beardall, J., Ralph, P., Heraud, P., 2013. Phenotypic plasticity of Southern Ocean diatoms: Key to success in the sea ice habitat? Ed. S. Lin. Plos ONE 8, e81185.
Schmidt, K., Brown, T.A., Belt, S.T., Ireland, L.C., Taylor, K.W.R., Thorpe, S.E., Ward, P., Atkinson, A., 2018. Do pelagic grazers benefit from sea ice? Insights from the Antarctic Sea ice proxy IPSO25. Biogeosciences 15, 1987–2006.
Schmidt-Rohr, K., 2015. Why combustions are always exothermic, yielding about 418 kJ per mole of O_2. J. Chem. Educ. 92, 2094–2099.
Sebastián, M., Smith, A.F., González, J.M., Fredricks, H.F., Van Mooy, B., Koblížek, M., Brandsma, J., Koster, G., Mestre, M., Mostajir, B., Pitta, P., Postle, A.D., Sánchez, P., Gasol, J.M., Scanlan, D.J., Chen, Y., 2016. Lipid remodelling is a widespread strategy in marine heterotrophic bacteria upon phosphorus deficiency. ISME J. 10, 968–978.
Stretch, J.J., Hamner, P.P., Hamner, W.M., Michel, W.C., Cook, J., Sullivan, C.W., 1988. Foraging behavior of antarctic krill Euphausia superba on sea ice microalgae. Mar. Ecol. Prog. Ser. 44, 131–139.
Subramanian, S., Barry, A.N., Pieris, S., Sayre, R.T., 2013. Comparative energetics and kinetics of autotrophic lipid and starch metabolism in chlorophytic microalgae: implications for biomass and biofuel production. Biotechnol. Biofuels 6, 150.
Tan, D., Ertunc, M.E., Konduri, S., Zhang, J., Pinto, A.M., Chu, Q., Kahn, B.B., Siegel, D., Saghatelian, A., 2019. Discovery of FAHFA-containing triacylglycerols and their metabolic regulation. J. Am. Chem. Soc. 141, 8798–8806.
Thomas, D.N., 2002. Antarctic Sea Ice–a habitat for extremophiles. Science 295, 641–644.
Trinh, R., Ducklow, H.W., Steinberg, D.K., Fraser, W.R., 2023. Krill body size drives particulate organic carbon export in West Antarctica. Nature 618, 526–530.
van Leeuwe M. A., Tedesco L., Arrigo K. R., Assmy P., Campbell K., Meiners K. M., Rintala J.-M., Selz V., Thomas D. N., Stefels J., 2018. Microalgal community structure and primary production in Arctic and Antarctic sea ice: a synthesis ed. J.W. Deming. Elementa: Sci. Anthropocene 6, 4.
Van Mooy, B.A.S., Fredricks, H.F., Pedler, B.E., Dyhrman, S.T., Karl, D.M., Koblížek, M., Lomas, M.W., Mincer, T.J., Moore, L.R., Moutin, T., Rappé, M.S., Webb, E.A., 2009. Phytoplankton in the ocean use non-phosphorus lipids in response to phosphorus scarcity. Nature 458, 69–72.
Wang, Q., Hou, Y., Miao, J., Li, G., 2009. Effect of UV-B radiation on the growth and antioxidant enzymes of Antarctic sea ice microalgae Chlamydomonas sp. ICE-l. Acta Physiol Plant 31, 1097–1102.
Wing, S.R., McLeod, R.J., Leichter, J.J., Frew, R.D., Lamare, M.D., 2012. Sea ice microbial production supports Ross Sea benthic communities: influence of a small but stable subsidy. Ecology 93, 314–323.
Zhang, H., Olson, D.J.H., Van, D., Purves, R.W., Smith, M.A., 2012. Rapid identification of triacylglycerol-estolides in plant and fungal oils. Ind. Crop. Prod. 37, 186–194.